The histone Lysine Methyltransferase 2D regulates pancreatic carcinogenesis through metabolic reprogramming

Marina Koutsioumpa[1], **Maria Hatziapostolou**[2,3], **Christos Polytarchou**[4], **Ezequiel J. Tolosa**[5], **Luciana L. Almada**[5], **Swapna Mahurkar-Joshi**[1], **Jennifer Williams**[6], **Belen Tirado-Rodriguez**[7], **Sara Huerta-Yepez**[7], **Dimitrios Karavias**[8], **Helen Kourea**[8], **George A. Poultsides**[9], **Kevin Struhl**[10], **David W. Dawson**[11], **Timothy R. Donahue**[6], **Martin E. Fernandez-Zapico**[5], **Dimitrios Iliopoulos**[1]

[1]Center for Systems Biomedicine, Vatche and Tamar Manoukian Division of Digestive Diseases, David Geffen School of Medicine, University of California at Los Angeles, Los Angeles, CA;

[2]Biological Sciences, University of Southampton, Southampton, United Kingdom;

[3]Biosciences, School of Science and Technology, Nottingham Trent University, Nottingham, United Kingdom;

[4]Interdisciplinary Biomedical Research Centre, School of Science and Technology, Nottingham Trent University, Nottingham, United Kingdom;

[5]Schulze Center for Novel Therapeutics, Division of Oncology Research, Mayo Clinic, Rochester, MN;

[6]Department of Surgery, Division of General Surgery, David Geffen School of Medicine at University of California Los Angeles, Los Angeles, CA;

[7]Unidad de Investigacion en Enfermedades Oncologicas, Hospital Infantil de Mexico, Mexico City, Mexico;

[8]Department of Pathology, School of Medicine, University of Patras, Patras, Greece;

[9]Department of Surgery, Stanford University School of Medicine, Stanford, CA;

[10]Department of Biological Chemistry and Molecular Pharmacology, Harvard Medical School, Boston, MA;

Correspondence to: Dimitrios lliopoulos, PhD MBA, Center for Systems Biomedicine, Vatche and Tamar Manoukian Division of Digestive Diseases, David Geffen School of Medicine, UCLA, 650 Charles E. Young Dr., CHS 44-133, Los Angeles, CA 90095-7278; iliopoulospharma@qmail.com.

[11]Department of Pathology and Laboratory Medicine, David Geffen School of Medicine at University of California Los Angeles, Los Angeles, CA.

Abstract

Objective: Despite advances in the identification of epigenetic alterations in pancreatic cancer, their biological roles in the pathobiology of this dismal neoplasm remain elusive. Here, we aimed to characterize the functional significance of histone lysine methyltransferases (KMTs) and demethylases (KDMs) in pancreatic tumorigenesis.

Design: DNA Methylation Sequencing and Gene Expression Microarrays were employed to investigate CpG methylation and expression patterns of KMTs and KDMs in pancreatic cancer tissues versus normal tissues. Gene expression was assessed in 5 cohorts of patients by qRT-PCR. Molecular analysis and functional assays were conducted in genetically modified cell lines. Cellular metabolic rates were measured using a XF24–3 Analyzer, while quantitative evaluation of lipids was performed by LC-MS analysis. Subcutaneous xenograft mouse models were used to evaluate pancreatic tumor growth *in vivo*.

Results: We define a new antitumoral function of the histone Lysine (K)-Specific Methyltransferase 2D (KMT2D) in pancreatic cancer. *KMT2D* is transcriptionally repressed in human pancreatic tumors through DNA methylation. Clinically, lower levels of this methyltransferase associate with poor prognosis and significant weight alterations. RNAi-based genetic inactivation of KMT2D promotes tumor growth and results in loss of H3K4me3 mark. In addition, KMT2D inhibition increases aerobic glycolysis and alters the lipidomic profiles of pancreatic cancer cells. Further analysis of this phenomenon identified the glucose transporter SLC2A3 as a mediator of KMT2D-induced changes in cellular metabolic and proliferative rates.

Conclusion: Together our findings define a new tumor suppressor function of KMT2D through the regulation of glucose/fatty acid metabolism in pancreatic cancer.

Keywords

Introduction

Emerging studies demonstrate that epigenetic rather than genetic changes modulate cancer phenotypes, in particular those controlling chromatin modifications such as histone methylation. In fact, there is evidence showing that changes in histone lysine methyltransferases (KMTs) and demethylases (KDMs), including KDM2B [1] and EZH2 [2] could affect pancreatic tumor growth. This is particularly important as it has been recently indicated that KMTs and KDMs could alter gene expression in a selective manner, while other chromatin modifiers, such histone deacetylases and DNA methyltransferases, globally regulate gene expression [3], Thus, understanding the function of histone methylation pathways could lead to a higher degree of specificity in targeting of specific epigenetic factors controlling pancreatic malignant transformation. In the present study, we provide evidence for a novel role for the histone Lysine (K)-Specific Methyltransferase 2 (KMT2D) in pancreatic carcinogenesis. Our ChlP-seq and genome wide gene expression

analysis, as well as, tumor growth studies strongly support its role as a pancreatic tumor suppressor in this disease. Specifically, KMT2D inhibition resulted in alterations of pancreatic cancer cells' bioenergetic and lipidomic profiles, by increasing aerobic glycolysis and lipids levels. Clinical outcomes across the range of body weight and Body Mass Index (BMI) were found to significantly correlate with KMT2D expression levels. Taken together, we have defined a previously uncharacterized function of KMT2D as growth limiting factor in pancreatic cancer and by mechanistic studies, we demonstrated that the metabolic reprogramming underlies this antitumoral function of KMT2D.

Materials and Methods

Cell Treatments

Cells were transfected with siRNAs for KMT2D, #1 (s15605) and #2 (s15604), SLC2A3 (S12933), LDLR (s224008), SLC2A1 (s12926), mTOR (s604), RICTOR (s226000) and control (4390846) using Lipofectamine RNAiMax transfection reagent (13778150, Life Technologies). Lentiviruses were produced in HEK293T cells (ATCC) transfected with the packaging and expression constructs using Fugene 6 (E2691, Promega). Cells were infected with the viruses using DEAE Dextran and selected with puromycin.

Mouse Experiments

Cells were transduced with shRNAs for KMT2D or scramble (1864, Addgene) lentiviral expressing constructs. Sequences containing the shRNAs for KMT2D:

#1–19: (sense:CCGGGAGTCGAACTTTACTGTCTCTGCAGAGACAGTAAAGTTCGACTCTTTTTG; antisense: AATTCAAAAAGAGTCGAACTTTACTGTCTCTGCAGAGACAGTAAAGTTCGACTC)

#2–19: (sense: CCGGCCACTCTCATCAAATCCGACTGCAGTCGGATTTGATGAGAGTGGTTTTTG; antisense: AATTCAAAAACCACTCTCATCAAATCCGACTGCAGTCGGATTTGATGAGAGTGG)

#1–21: (sense, CCGGGAGTCGAACTTTACTGTCTCCCTGCAGGGAGACAGTAAAGTTCGACTCTTTTTG; antisense, AATTCAAAAAGAGTCGAACTTTACTGTCTCCCTGCAGGGAGACAGTAAAGTTCGAC

#2–21: (sense, CCGGCCACTCTCATCAAATCCGACACTGCAGTGTCGGATTTGATGAGAGTGGTTTTTG; antisense, AATTCAAAAACCACTCTCATCAAATCCGACACTGCAGTGTCGGATTTGATGAGAGGG)

were annealed and cloned into the pLKO.1 puro (8453, Addgene) vector according to the Janes Lab protocol (http://bme.virginia.edu/janes/protocols/pdf/Janes_shRNAcloning.pdf). $3.5*10^6$ or $4.5*10^6$ MIA PaCa-2 and CAPAN-2 cells were injected subcutaneously in the right flank of NOD-SCID mice (5 mice/group). Tumor volume was monitored every week for up to 84 days, respectively. Tumor volumes were calculated by the equation V (mm^3) = axb^2/2, where a is the largest diameter and b is the perpendicular diameter. Bars represent means ± SD.

Data Availability Section:

Array and Sequencing data have been deposited in the Gene Expression Omnibus (GEO) database (http://www.ncbi.nlm.nih.gov/geo/). Gene Expression Array, Targeted Bisulfite Sequencing and ChIP-seq data are available under the following accession numbers GSE85991, GSE85961 and GSE85886, respectively.

Additional Materials and Methods are included as part of the Supplementary Materials and Methods section.

Results

KMT2D exerts tumor suppressive activities in pancreatic cancer

In order to define the role of KMTs and KDMs in pancreatic carcinogenesis, we initially determined the levels of these enzymes in tumors (n=14) and adjacent controls (n=8) and found different members of the KDM family (*KDM2A, KDM4C, KDM5B, KDM8), SETD* family (*SETDB2, SETD6*), the *SUV420H1* and *KMT2D* to be differentially expressed (Supplementary Table S1). As shown in Figure 1A and Supplementary Figure S1A, statistically significant and consistent deregulation of gene expression was observed only for *KMT2D* in 3 independent patient Cohorts. We further investigated the differential *KMT2D* expression based on previously published gene expression array data listed in the Oncomine™ database. Notably, KMT2D mRNA expression also displays significantly decreased levels based on 2 independent studies [4 5] (Supplementary Figure S1B–C). The expression of other H3K4 methyltransferase genes sharing similar structural domains with *KMT2D* was also measured. As shown in Supplementary Figures S1D–E, no significant changes were observed in the mRNA levels of neither *KMT2B* nor *KMT2C* in the human pancreatic cancer samples used in the current study.

Based on the above findings we postulated the hypothesis that KMT2D might display tumor suppressive properties in pancreatic cancer. To address this hypothesis, we performed a series of *in vitro* and *in vivo* experiments where KMT2D was genetically inactivated, as evidenced in Figure 1B. Transient downregulation of *KMT2D* by using 2 different siRNAs promoted cellular proliferative capacity (Figure 1C, Supplementary Figure S1F–G and Supplementary Tables S2–3). To confirm the biological significance of KMT2D, pancreatic cancer cells stably suppressed of KMT2D expression were established (Supplementary Figure S1H) and tested for their proliferative capacity (Supplementary Figures S1I–L). The most efficient shRNA-transfected cell population (#2–21) was subjected to clonal selection and used for the further studies. Quantitative Reverse Transcription Polymerase Chain

Reaction (RT-qPCR) and immunoblot (IB) analysis were used to verify the lower levels of KMT2D mRNA and protein in the clonal cell lines (Figure 1D). Similar to transient knockdowns, stably decreased KMT2D expression led to increased MIA PaCa-2 proliferation (Figure 1E, Supplementary Figure S1M–N and Supplementary Table S4–5) and cell anchorage-independent growth (Figure 1F and Supplementary Figure S1O).

To further validate our hypothesis, the effects of KMT2D inhibition of expression were investigated in nude mice bearing human pancreatic cancer xenografts. Significant induction of tumor growth rate and weight was observed (Figure 1G-H and Supplementary Figures S1P–Q) and lower KMT2D mRNA levels were confirmed by RT-qPCR and immunohistochemical (IHC) analysis (Supplementary Figures S1R–S) in the excised tumors. Consistent with these observations, histopathological analysis of tumors from different mice at the endpoint revealed high proliferation rates, as evidenced by Ki-67 Immunostaining (Figure 1I). Taken together, these *in vitro* and *in vivo* results, point towards a tumor suppressive role of KMT2D in pancreatic cancer.

Site-specific DNA methylation associates with *KMT2D* transcriptional repression

We next sought to determine the mechanism underlying KMT2D decreased expression in pancreatic cancer. To this end, we designed a complementary tissue- and cell-based experimental approach for the evaluation of *KMT2D* transcriptional repression-dependency on DNA methylation, as depicted in Figure 2A. We investigated DNA methylation patterns of KMTs and KDMs in 20 pancreatic cancer tissues compared with 13 adjacent control tissues by using the Infinium Human Methylation 450 Bead ChIP Array. *KMT2D*, together with other four of these enzymes, was found to be significantly differentially methylated (at least over 25%) in pancreatic tumors compared to normal tissues (Figure 2B and Supplementary Table S6). Specifically, methylation of 2 individual CpG motifs was observed at nucleotides (nt) −29 and +45, relatively to the *KMT2D* transcription start site (TSS). By integrating the data originating from CpG methylation genome-wide analysis with gene expression profiling in cancerous versus normal pancreas, KMT2D was simultaneously identified to be aberrantly hypermethylated and downregulated. Whole Exome Sequencing in the pancreatic cancer cell lines used in the current study (Table S7), as well as published data from other groups show that *KMT2D* harbors deletions and mutations in pancreatic ductal adenocarcinoma (PDAC), however the actual frequencies of such mutations in PDAC are still debatable [6 7], In addition, the phenotypic consequences of such mutations, have not yet been assessed in any disease setting. Given the above, we cannot rule out the possibility that genetic inactivation of *KMT2D* relies partly on both its mutational-and/or CpG methylation-status.

Next, targeted bisulfate sequencing was performed for the specified region comprising of nt: −179 to +122, in a panel of 5 pancreatic cancer cell lines treated with the DNA methyltransferase inhibitor 5-AZA-2'-deoxycytidine (5-AZA-CdR, Decitabine). Box plots of DNA methylation levels indicate that drug-treated cells have an extensive hypomethylated pattern (Figure 2C and Supplementary Figure S2A). Further evidence on the impact of CpG methylation to repress *KMT2D* transcriptional activity were obtained from analysis of KMT2D mRNA levels upon different exposure times and concentrations of the drug (Figure

2D and Supplementary Figure S2B). The most robust time- and dose-dependent changes occurred in MIA PaCa-2 and AsPC-1 cell lines, an observation that was further validated by IB analysis (Figure 2E). However, since this agent induces genome-wide demethylation, the observed increase in expression after treatment could be indirect. To eliminate this possibility, we designed a luciferase reporter assay for *in vitro* methylated *KMT2D* genomic region of interest (ROI) in wild type or mutated state (Figure 2F). Linearized constructs were *in vitro* methylated with high efficiency, as evidenced by resistance to digestion with Hpall methylation-specific endonuclease (Figure 2G). As proof-of-concept, no significant differences were found among the promoter activity of unmethylated inserts (serving as positive controls), while in the totally unmodified methylated insert *Renilla luciferase reporter gene (hRluc)* activity was almost absent, thus confirming that CpG methylation controls transcriptional repression of *KMT2D*. Remarkably, both mutations applied in the ROI seem to derepress the *hRluc* activity of the *in vitro* methylated constructs by approximately 22-or 12-fold for Mut 1 and Mut 2, respectively (Figures 2H and I). Taken together, our results identified that single-site CpGs methylation is critical for the suppression of KMT2D expression levels in pancreatic cancer.

KMT2D depletion promotes a metabolic shift to aerobic glycolysis through regulation of SLC2A3

Next, we investigated the mechanisms downstream of KMT2D underlying its tumor suppressor functions. KMT2D belongs to the COMPASS family of H3K4 methyltransferases [8], thus, we first examined the effects of KMT2D on global H3K4 methylation marks in pancreatic cancer cells. Using IB we showed that H3K4 mono- and di-methylated were slightly downregulated in the siKMT2D-treated cells, while the tri-methylated form of H3K4 (H3K4me3) was significantly reduced (Figure 3A). Furthermore, we tested the effect of 5-AZA-CdR treatment, as a means to overexpress KMT2D, on the H3K4me3 levels of pancreatic cancer cells. Consistent with the notion that H3K4 methylation is enriched upon 5-Aza-dCdR treatment, potentially as a secondary event following the promoter demethylation and gene reexpression [9 10], we observed a remarkable enrichment of H3K4me3 methylation upon agent treatment. Interestingly, silencing of KMT2D in 5-Aza-dCdR-treated cells did not decrease H3K4me3 methylation levels as efficiently as in untreated cells, most possibly due to higher KMT2D levels (Supplementary Figure S3A and S3B), while non-significant alterations in H3K4me1/2 levels were observed (Supplementary Figure S3C). To complement these initial findings, chromatin immunoprecipitation-sequencing (ChlP-seq) analysis for H3K4me3 and microarray gene expression profiling were performed in MIAPaCa-2 cells. ChlP-seq analysis showed significant decrease in H3K4me3 signals in KMT2D-silenced versus non-targeting control cells (Figure 3B). The H3K4me3 peaks significantly overlap between the 2 different siRNAs used, as shown by the Venn diagram (Figure 3C). H3K4me3 peaks were associated mostly with intergenic and intronic regions and were located around the TSS site (Figures 3D and E). Marked loss of H3K4me3 peaks also occurs in loci essential for gene transcription as in the case of the *General Transcription Factor IIA Subunit 1 (GTF2A1)*, a component of the transcription machinery of RNA polymerase II that plays an important role in transcriptional activation (Supplementary Figure S4). Gene Ontology (GO) analysis of the H3K4me3 peaks found to be diminished upon *KMT2D* silencing identified

association with transcription-related pathways, with the highest enrichment score being observed for "transcription from RNA polymerase II promoter" and metabolic processes (Figure 3F). *Serine/Threonine Kinase 11 (STK11)* represents an example of KMT2D-mediated regulation of metabolic gene through reduction of H3K4me3 occupancy that was further experimentally validated as a direct regulatory target of KMT2D (Supplementary Figure S5). Gene expression studies demonstrated 1035 genes to be down regulated, while a smaller subset of genes was upregulated upon KMT2D suppression (Figure 3G). We mapped the differentially regulated genes to well established ("canonical") pathways by using Ingenuity Pathway Analysis Software (IPA) (Ingenuity Systems, http://www.ingenuity.com/). Energy-converting biochemical processes, primarily related to glucose and fatty acid (FA) metabolism, were distinguished as KMT2D-mediated cellular functions (Figure 3H). Collectively, both the ChIP-seq and microarray studies pointing to the association of KMT2D expression with metabolism-related pathways.

To further explore the functional consequences of the metabolism-associated KMT2D target(s) we measured changes of nicotinamide adenine dinucleotide phosphate (NADPH), that represents a fundamental common mediator of various biological processes including energy metabolism [11], We found that cells harboring low KMT2D levels accumulate higher NADPH levels in comparison to control cells (Supplementary Figure S6A). Given this observation, we reasoned to assay cultured cells in real time using a XF24–3 Analyzer to query changes in the bioenergetic status of KMT2D-suppressed versus control pancreatic cancer cells. Simultaneous assessment of both Oxygen Consumption Rate (OCR) and Extracellular Acidification Rate (ECAR) in basal state showed enhanced relative contribution of glycolysis upon *KMT2D* suppression (Figure 3I and Supplementary Figure S6B–C). In particular, significant increase in ECAR values was observed, while OCR seems to remain unaffected, thus augmenting cellular preference for aerobic glycolysis. By quantifying the activity of the two major energy-yielding pathways in the cell, mitochondrial respiration and glycolysis, we provide evidence of a clear discrimination in the metabolic profiles driven by loss of KMT2D expression. Furthermore, lactate production as well as glucose uptake, were found to be significantly elevated upon KMT2D silencing (Supplementary Figure S6D–G).

In light of the above results, we hypothesized that KMT2D could influence glucose metabolism by controlling key glycolytic genes. Expression of the SLC2A1 (Glucose transporter-1 (GLUT-1)) that typically correlates with the rate of cellular glucose metabolism was found to be merely upregulated (+1.25 fold change) in *KMT2D*-silenced cells (Figure 4A) and was not significantly affected in the tumors originating from xenografts bearing KMT2D stably-suppressed pancreatic cancer cells (Supplementary Figure S7). Of note, *Solute Carrier Family 2 Member 3 (SLC2A3)*(also known as *GLUT3*) was distinguished as the top differentially expressed glycolysis-related gene upon KMT2D downregulation (Figure 4A-C and Supplementary Figure S8). To rule out secondary effects related to the genetic status of *SLC2A3* in the 2 different pancreatic cancer cell lines, we demonstrate that mostly common single nucleotide changes of *SLC2A3* gene are observed, all of them ensuing synonymous substitutions (Supplementary Table S8). Mapped DNA sequence reads from the ChIP-seq experiments mentioned above, do not support the role of

SLC2A3 as a direct KMT2D transcriptional target. Hence, we assessed whether KMT2D transcriptionally regulates *SLC2A3* through an indirect effect.

Tuberous sclerosis 1 (TSC) 1 that acts as upstream negative regulator of mTOR activation [12], was found to be significantly downregulated based on the gene expression array employed in KMT2D-supressed cells (Figure 3G). In addition, by pharmacological or genetic strategies it has been demonstrated that rapamycin-sensitive mTOR complex 1 (mTORC1), consisting of mTOR itself and the regulatory-associated protein of mTOR (Raptor), is involved in the regulation of SLC2A3 expression. Specifically, loss of the TSC1 induced mTOR hyperactivation and SLC2A3 overexpression through the activation of the IKK/nuclear factor kappa-light-chain-enhancer of activated B cells (NF-κB) pathway [13]. In another report, stimulation of NF-kB activity has also been shown to directly upregulate *SLC2A3* gene transcription in mouse and human cells [14]. Indeed, IB analysis shows that reduction of *KMT2D* expression leads to increased phosphorylation and thus activation of mTOR (Figure 4D) and increased phosphorylation of NF-kB p65 in Ser 536 (Figure 4E). On the other hand, the expression of REL-associated protein (p65) involved in NF-kB heterodimer formation, nuclear translocation and activation, is not influenced upon *KMT2D* genetic manipulation (Supplementary Figure S9). Silencing of *mTOR*, but not *Rictor* (a specific component of mTORC2), as well as rapamycin treatment reverse the SLC2A3 upregulation that is induced by low KMT2D levels (Figure 4F and Supplementary Figure S10). Furthermore, the use of inhibitors of NF-kB activation resulted in the partial reversal of SLC2A3 mRNA levels induction caused by *KMT2D* silencing (Figure 4G). These data suggest that KMT2D suppression promotes SLC2A3 expression via activation of the mTOR/NF-κB axis. The Immunostaining patterns of activated NF-κB p65 and SLC2A3 in tumors from xenografts bearing KMT2D stably-suppressed or mock-transfected MIA PaCa-2 cells (Supplementary Figure S11) validated our *in vitro* findings. Most importantly, treatment of pancreatic cancer cells with siRNA for SLC2A3 rescues the metabolic (Figure 4H), proliferative (Figure 4I) and Supplementary Tables S9–10 and anchorage independent growth phenotype (Figure 4J), that is associated with KMT2D suppression. Collectively, the functional features displayed by SLC2A3 reduction in KMT2D-low expressing cells highlight its role as a mediator of KMT2D-induced effects.

Polyunsaturated fatty acids are increased in KMT2D-suppressed cells and promote cell growth time-dependently

It is now considered that cancer cells support their increased growth rate by increasing either the uptake of exogenous lipids or their endogenous synthesis [15]. Functional enrichment analysis (Figure 5A), as well as bioinformatics prediction of the top-rated pathways and networks (Figure 3G and Supplementary Table S11) of differentially expressed genes in KMT2D-silenced cells, suggest that KMT2D expression has an impact on lipid metabolic processes. Genes found in the particular functional cluster are illustrated in Figure 5B and among those, *Fatty acid synthase (FASN)* that encodes a multi-enzyme protein catalyzing fatty acid synthesis, is one of the top differentially regulated genes upon *KMT2D* downregulation (Supplementary Figure S12). Interestingly, we noticed that MIA PaCa-2 and CAPAN-2 bearing xenografts exhibit a clear trend of increased body weight, mainly at prolonged stages of tumor growth (Figure 5C and Supplementary Figure S13), even though

these mice were possibly expected to be of poorer health given their increased tumor burden. However, the increase in the overall body weight of the mice most possibly relates to the increased weight of the tumors

As a next step, we used mass spectrometry-based technology to assess quantitative changes in FA composition and cholesterol content as a response to KMT2D silencing. Specifically, the total number of lipid species identified accounts for 28 FAs, all of which displayed increased levels relative to control cells (Table 1), with the most prominent differences being observed for the polyunsaturated fatty acids (PUFAs) docosadienoic, docosatrienoic and docosatretraenoic (Table 1 and Figure 5D).

Interestingly, addition of the aforementioned lipids in serum free conditions resulted in increased MIA PaCa-2 cell growth in a time- and dose-dependent manner (Figure 5E) but did not affect pancreatic cancer cell's invasive capacity (Supplementary Figure S14). Furthermore, elevated cholesterol uptake was detected in MIA PaCa-2 cultured cells transiently transfected with a siRNA against KMT2D, as assessed by fluorescence microscopy (Figure 5F). Subsequently, we explored whether cells harboring low or high KMT2D levels differentially respond to perturbations in lipid homeostasis by a) silencing the low density lipoprotein receptor (LDLR), the main selective route of cholesterol-rich lipoprotein entrance into cancer cells b) blocking the ATP citrate lyase (ACLY), a critical enzyme for *de novo* synthesis of a wide range of complex cellular lipids such as cholesterol and long-chain FAs using the SB 204990 inhibitor and c) blocking the 6 desaturase, the rate-limiting enzyme that initiates the metabolism of the n-6 and n-3 PUFAs, linoleic acid and α-linolenic acid respectively, into their downstream long chain FA conversion products using the selective SC 26196 inhibitor. We found that reduction in MIA PaCa-2 cell proliferation rate caused by lipid synthesis/uptake blockage is more pronounced in cells lacking KMT2D expression, with the maximum effect among the compounds used being observed in the case of the selective 6 desaturase inhibitor SC 26196 (Figure 5G). The latter result substantiates the functional importance of the top KMT2D-regulated lipids in pancreatic cancer, since the SC 26196 compound inhibits the rate-limiting step in arachidonic acid synthesis pathway, in which both docosadienoic and docosatetraenoic acids are implicated. Overall, these results revealed that the cellular lipid profiles depend on KMT2D expression. Furthermore, we are the first ones to show the potential of docosadienoic, docosatrienoic and docosatretraenoic acids to promote growth of pancreatic cancer cells, as evidenced by time-dependent studies.

Synergistic role of glycolytic and lipidomic effectors in KMT2D-related phenotype

Lipogenic phenotype (characterized by increased FA synthesis, lipids' uptake and metabolism) has been functionally and temporally linked to the glycolytic metabolism in primary and metastatic cancers as essential interaction regulating the malignant phenotype [16]. Thus, we explored whether KMT2D-mediated impact on cancer cell proliferation is interdependent on both glucose/lipid metabolism-related downstream effectors. Notably, combined treatment of cells with a siRNA for SLC2A3 and the SC 26196 inhibitor completely reversed the effect of *KMT2D* depletion in MIA PaCa-2 cell proliferation (Figure 5H), thus indicating the synergistic role of both SLC2A3 expression and

maintenance of proper lipid composition as mediators of KMT2D-induced proliferative phenotype.

Clinical relevance of the KMT2D expression in pancreatic cancer

To define the clinical relevance of our findings, KMT2D expression was examined by IHC and quantitative automated image analysis in matched adjacent control-cancerous tissues from 26 pancreatic cancer patients (Cohort IV). KMT2D staining patterns showed that its nuclear localization is almost absent in tumor samples, while highly expressed in normal tissues (Figure 6A and Supplementary Figure S15A). Further analysis of KMT2D expression in subgroups reflecting Stage I or II of pancreatic cancer patients (Cohort IV) shows that the decrease in KMT2D levels may be significant in more advanced stages of the disease (Supplementary Figure S15B). However, whether KMT2D levels relate to disease progression needs to be further explored in extended numbers of human biopsies and genetically engineered mouse models of pancreatic cancer. Kaplan-Meier analysis performed in 158 cases (Cohort V) and in 22 cases (Cohort III), revealed that pancreatic cancer patients harboring low *KMT2D* expression levels had worse prognosis in comparison with patients harboring high KMT2D levels (Figure 6B and Supplementary Figure S16). Sample power calculations conducted for the larger Cohort V suggest that an extended sample size (over 2,800 cases) is needed to reach statistical significance (Supplementary Table S12). It should be highlighted that the samples derived from Cohort V reflect mostly (90%) Stage II cases, thus rendering it very difficult to detect survival differences with statistical significance. On the other hand, 86% of the tumors derived from Cohort III reflect Stage III pancreatic cancer patients. Subsequently, we conducted correlation analysis for the levels of KMT2D with its downstream effectors. Expectedly, the Pearson coefficients computed reflect a negative correlation between KMT2D and SLC2A3 mRNA levels (Figure 6C and D), based on publicly available gene expression array data and our experimental RT-qPCR validation studies. Significantly, IHC analysis of activated NF-kB p65 and SLC2A3 in matched adjacent control-cancerous tissues shows increased Immunostaining of both in the tumor-derived samples where KMT2D protein levels were found to be very low compared to normal samples. These results further validate our *in vitro* mechanistic findings that suggest KMT2D-dependent NF-kB activation and thus, SLC2A3 upregulation in pancreatic cancer.

Correlation of *KMT2D* expression with various clinical parameters is illustrated in Table 2 and Supplementary Table S13.

No significant association was observed between *KMT2D* expression and age ($P=.4976$), sex ($P=.2999$) or race ($P=.3702$). Interestingly, patients with high KMT2D levels display dramatic weight loss and higher BMI values with high statistical significance. Out of 106 cases with above median (>3.917) *KMT2D* expression, 84 (79.2%) cases lost an average of 20.65 pounds. On the other hand, a significant correlation of *KMT2D* expression was further observed in 95 cases with increased body fat, as assessed by BMI measurements. In our attempt to address whether biopsies derived from patients harboring low KMT2D levels exert quantitative changes in FA composition and cholesterol content relatively to control tissues, we performed Lipidomics Analysis in samples derived from Cohort II. Remarkably,

we found that among the top lipids being robustly upregulated with statistical significance in human biopsies are docosadienoic, docosatrienoic and docosatretraenoic acids, thus validating our *in vitro* results showing dramatic increase of these PUFAs upon genetic inactivation of *KMT2D* in pancreatic cancer cells (Table 3).

Overall, these findings support the relevance of KMT2D for human pancreatic carcinogenesis. Figure 7 shows a diagram illustrating the upstream and downstream effectors of KMT2D expression and activity in pancreatic cancer.

Discussion

Novel role for the KMT2D-H3K4me axis in pancreatic cancer

Studies illustrating the role of KMT2D in histone H3K4 methylation at enhancers [17] or in the maintenance of genome stability in genes [18] help rationalize its widespread role in tumorigenesis. Based on a somatic knockout of KMT2D in human cells, microarray analysis revealed that a subset of genes that were associated with KMT2D-enriched loci displayed reduced expression in KMT2D-depleted cell lines that was accompanied by reduced H3K4me3 [19]. Recent research focus indicates the direct connections between metabolism and chromatin dynamics, underlying many aspects of metabolic dysfunction. Interestingly, KMT2D-Activating signal cointegrator-2 complex has been shown to play redundant but essential roles in ligand-dependent H3K4me3 and expression of Liver X receptor-target genes [20] and peroxisome proliferator-activated receptor gamma-dependent adipogenesis [21] and hepatic steatosis [22].

Here, by analyzing pathways derived from H3K4me3 regions we identified an association of KMT2D expression with metabolic processes. Our ChIP-seq data and mechanistic experiments support that *STK11* represents a direct regulatory target of KMT2D. Noteworthy, several groups suggest that STK11 role as a master regulator of polarity and metabolism contributes to its tumor suppressor function [23 24], Beyond that, our ChIP-Seq data show that several transcription factors' loci exhibit significantly reduced H3K4me3 occupancy in KMT2D-silenced cells. Interestingly, it has been reported that focal rather than global loss of the H3K4me1/me2 marks has been observed at putative enhancers in mouse KMT2D-depleted lymphomas and among the genes with concurrent expression changes were tumor suppressor genes [25]. In the present study, we did not explore H3K4me1 and H3K4me2 abundance upon KMT2D silencing, since global loss of the marks genome wide was not observed in pancreatic cancer cells. However, the possibility of H3K4me1/me2 enrichment loss upon KMT2D silencing in a focal manner could not be excluded. These data point to the complexity of a gene network contributing to the KMT2D-related metabolic phenotype of pancreatic cancer cells, either by the direct action of metabolic genes and/or by the secondary effects induced by transcription factors.

Importance of SLC2A3 glucose transporter in pancreatic cancer

Many studies have reported oncogenic aberrations of key glycolytic enzymes that mechanistically stimulate activation of glucose uptake [26], SLC2A1 (Glucose transporter-1 (GLUT-1)) is a member of the GLUT family of facilitative glucose transporters that

accounts for the uptake of glucose by malignant cells to a high extent. It is overexpressed in a wide range of human cancers, including pancreas [27], and forced overexpression of SLC2A1 has been shown to induce pancreatic cancer cellular invasiveness [28], However, in pancreatic cancer cells and xenografts harboring low KMT2D levels minor changes in *SLC2A1* levels were observed, while very significant alterations were found in *SLC2A3* expression. In particular, we found induction of the *SLC2A3* glucose transporter triggered by KMT2D suppression, the former mediating the effect of KMT2D on cellular metabolism and proliferation. SLC2A3 displays a high affinity for glucose thus ensuring efficient glucose uptake [29], however its expression is very low or undetectable in most organs of healthy adults. Of note, the impact of SLC2A3 levels on the stimulation of brain tumor initiating cells' growth has been recently demonstrated [30] and pathological SLC2A3 overexpression has been reported in pancreatic cancer [31]. In this realm, we now unveil a novel mechanism where the epigenome regulates the glycolytic profile of pancreatic cancer cells via SLC2A3 regulation.

Disease relevance for KMT2D-regulated pathways

The biological findings reported in the literature suggest a cell type or context dependent functional role of KMT2D in cancer. Impairment of cellular growth and invasion in breast cancer mouse xenografts, as well as in human colorectal and medulloblastoma cell lines, has been attributed to KMT2D knockdown [32 33], On the other hand, Lee and colleagues showed that KMT2D interacts directly with p53 to promote expression of p53 target genes [34], Remarkably, its early loss has been shown to facilitate lymphomagenesis by remodeling the epigenetic landscape of the cancer precursor cells [35], Our study supports that KMT2D restrains pancreatic cancer growth through the regulation of metabolic pathways. However, the study of Dawkins *et al.*, 2016, focusing on the impact of H3K4 methyltransferases KMT2C and KMT2D in pancreatic adenocarcinoma biology points towards an oncogenic role for KMT2D. Specifically, transient knockdown of KMT2D in a panel of pancreatic cancer cell lines resulted in growth inhibition [36]. In our study KMT2D expression was stably blocked by 4 different shRNA sequences, thus evaluating the long-term effects of KMT2D inhibition of expression. The latter provides confidence for the specificity of the KMT2D-induced functional effects. Moreover, we performed real-time cell proliferation analysis based on the application of electrical cell substrate impedance changes method, which exhibits many advantages over the conventional endpoint assays for monitoring cell proliferation. Beyond the differences in the technical set-up, acquisition or loss of mutations by cancer cell lines could not be excluded. Nonetheless, the functional effects of KMT2D are supported by our mechanistic studies, showing that the genomic, glycolytic and lipidomic changes caused by KMT2D suppression refer and relate to a status of increased bioenergetic needs of proliferating cells. Furthermore, silencing of KMT2D causes significant alterations on the expression levels of genes with well-established role(s) in the biosynthesis, beta-oxidation, degradation or uptake facilitation of lipids, such as *FASN, ACACA, LIPA* and *HMGCR. FASN*, that was distinguished among the top differentially regulated genes upon KMT2D down regulation, is essential for catalyzing the formation of palmitate from acetyl-coenzyme A and malonyl-coenzyme A in the presence of NADPH, thus controlling the FAs biosynthesis [37], It is considered a viable candidate as indicator of pathologic state, marker of neoplasia, as well as, pharmacological treatment

target in pancreatic cancer [38 39], In our *in vitro* experimental setting, FASN upregulation triggering increased FA synthesis possibly accounts for the moderate increase in palmitic acid levels, which is the first FA produced during FA synthesis and is the precursor to longer FAs. However, this finding was not validated in pancreatic cancer patients (Cohort III), as assessed by correlation analysis or KMT2D/FASN mRNA levels (data not shown). This discrepancy could possibly be attributed to the small sample size used, which may not be adequate to detect significant correlations and/or the diversity of the genetic/epigenetic patterns and other features of human pancreatic tumors. Nonetheless, since a broader network of lipid-related genes is affected in KMT2D-suppressed pancreatic cancer cells, the extent to which distinct pathways such as lipid synthesis/degradation/metabolism or efflux contribute to the phenotype of altered lipid profiles is currently under further investigation.

Interestingly, by using adipogenesis as a synchronized model of cell differentiation, it has been previously indicated that KMT2D exhibits cell type- and differentiation stage-specific genomic binding and is predominantly localized on enhancers. These data suggest a step wise model of enhancer activation during adipogenesis that includes cooperative recruitment of KMT2D to perform H3K4me1/2 on enhancer-like regions by lineage-determining transcription factors, such as C/EBPβ, PPARγ and C/EBPα [17]. In accordance to the concept of KMT2D as a component of genetic regulation that affects adipose/lipid homeostasis, our human data point out that patients harboring high KMT2D expression experience greater weight loss and higher BMI, than patients whose KMT2D levels are below the median value. The sample size of Cohort V did not have enough power to define survival differences; however, there was a trend of increased survival in patients with higher levels of KMT2D. Discordance with the study of Dawkins *et al.*, showing that reduced expression of *KMT2D* correlates with improved outcome in PDAC, most possibly arises due to sample type differences, especially given that Cohort V consists of samples from resected (Stage II) cases. It has been documented that not only the degree of weight loss impacts survival of pancreatic cancer patients, but also the proportion of muscle and fat loss in the different compartments [40]. Fat oxidation, decreased lipogenesis, impaired lipid deposition/adipogenesis and mainly elevated lipolysis have been linked to fat loss, however the underlying mechanisms have not been clearly defined [41]. It is tempting to speculate that KMT2D expression may account for body weight and composition changes during illness progression, as a factor causing alterations in glucose/lipid/ metabolism.

Taken together, our experimental strategy has revealed the mechanisms that regulate KMT2D expression and its downstream effectors in pancreatic oncogenesis. The present study offers significant mechanistic value for potential treatment of pancreatic cancer as a metabolic disease regulated by the epigenome.

Supplementary Material

Refer to Web version on PubMed Central for supplementary material.

Acknowledgements:

Abbreviations:

2-DG	2-deoxyglucose
5-AZA-CdR	5-AZA-2'-deoxycytidine
BMI	Body mass index
ChIP-seq	chromatin immunoprecipitation-sequencing
DNMTs	DNA methyltransferases
ECAR	Extracellular Acidification Rate
FA	fatty acid
FASN	fatty acid synthase
GO	gene ontology
H3K4	histone H3 lysine 4
H3K4me1	mono-methylated form of H3K4me levels
H3K4me2	di-methylated form of H3K4me levels
H3K4me3	tri-methylated form of H3K4me levels
hRluc	renilla luciferase
IB	immunoblot
IHC	immunohistochemical
IPA	Ingenuity Pathway Analysis software
KDMs	histone lysine demethylases
KMT2D	lysine (K)-specific methyltransferase 2D
KMTs	histone lysine methyltransferases
Luc	firefly luciferase
NADPH	nicotinamide adenine dinucleotide phosphate
NF-κB	nuclear factor kappa-light-chain-enhancer of activated B cells
nt	nucleotide
OCR	oxygen consumption rate

PUFAs	omega-3-polyunsaturated fatty Acids
ROI	region of interest
RT-qPCR	quantitative reverse transcription polymerase chain reaction
SLC2A1	Solute Carrier Family 2 Member 1
SLC2A3	Solute Carrier Family 2 Member 3
STK11	Serine/Threonine Kinase 11
TSGs	tumor suppressor genes
TSS	transcription start site

References

1. Tzatsos A, Paskaleva P, Ferrari F, et al. KDM2B promotes pancreatic cancer via Polycomb-dependent and -independent transcriptional programs. J Clin Invest 2013;123(2):727–39 doi: 10.1172/jci64535[published Online First: Epub Date]|. [PubMed: 23321669]

2. Mallen-St Clair J, Soydaner-Azeloglu R, Lee KE, et al. EZH2 couples pancreatic regeneration to neoplastic progression. Genes Dev 2012;26(5):439–44 doi: 10.1101/gad.181800.111[published Online First: Epub Date]|. [PubMed: 22391448]

3. Kubicek S, Gilbert JC, Fomina-Yadlin D, et al. Chromatin-targeting small molecules cause class-specific transcriptional changes in pancreatic endocrine cells. Proc Natl Acad Sci U S A 2012;109(14):5364–9 doi: 10.1073/pnas.l201079109[published Online First: Epub Date]|. [PubMed: 22434908]

4. Badea L, Herlea V, Dima SO, Dumitrascu T, Popescu I. Combined gene expression analysis of whole-tissue and microdissected pancreatic ductal adenocarcinoma identifies genes specifically overexpressed in tumor epithelia. Hepato-gastroenterology 2008;55(88):2016–27 [PubMed: 19260470]

5. Segara D, Biankin AV, Kench JG, et al. Expression of HOXB2, a retinoic acid signaling target in pancreatic cancer and pancreatic intraepithelial neoplasia. Clinical cancer research : an official journal of the American Association for Cancer Research 2005;11(9):3587–96 doi: 10.1158/1078-0432.ccr-04-1813[published Online First: Epub Date]|. [PubMed: 15867264]

6. Sausen M, Phallen J, Adleff V, et al. Clinical implications of genomic alterations in the tumour and circulation of pancreatic cancer patients. Nature communications 2015;6:7686 doi: 10.1038/ncomms8686[published Online First: Epub Date]|.

7. Bailey P, Chang DK, Nones K, et al. Genomic analyses identify molecular subtypes of pancreatic cancer. Nature 2016;531(7592):47–52 doi: 10.1038/naturel6965[published Online First: Epub Date]|. [PubMed: 26909576]

8. Ruthenburg AJ, Allis CD, Wysocka J. Methylation of lysine 4 on histone H3: intricacy of writing and reading a single epigenetic mark. Mol Cell 2007;25(1):15–30 doi: 10.1016/j.molcel.2006.12.014[published Online First: Epub Date]|. [PubMed: 17218268]

9. Fahrner JA, Eguchi S, Herman JG, Baylin SB. Dependence of histone modifications and gene expression on DNA hypermethylation in cancer. Cancer research 2002;62(24):7213–8 [PubMed: 12499261]

10. Si J, Boumber YA, Shu J, et al. Chromatin remodeling is required for gene reactivation after decitabine-mediated DNA hypomethylation. Cancer research 2010;70(17):6968–77 doi: 10.1158/0008-5472.can-09-4474[published Online First: Epub Date]|. [PubMed: 20713525]

11. Ying W NAD+/NADH and NADP+/NADPH in cellular functions and cell death: regulation and biological consequences. Antioxidants & redox signaling 2008;10(2):179–206 doi: 10.1089/ars.2007.1672[published Online First: Epub Date]|. [PubMed: 18020963]

12. Zhang H, Bajraszewski N, Wu E, et al. PDGFRs are critical for PI3K/Akt activation and negatively regulated by mTOR. The Journal of clinical investigation 2007;117(3):730–8 doi: 10.1172/jci28984[published Online First: Epub Date]|. [PubMed: 17290308]

13. Zha X, Hu Z, Ji S, et al. NFkappaB up-regulation of glucose transporter 3 is essential for hyperactive mammalian target of rapamycin-induced aerobic glycolysis and tumor growth. Cancer letters 2015;359(1):97–106 doi: 10.1016/j.canlet.2015.01.001[published Online First: Epub Date]|. [PubMed: 25578782]

14. Kawauchi K, Araki K, Tobiume K, Tanaka N. p53 regulates glucose metabolism through an IKK-NF-kappaB pathway and inhibits cell transformation. Nature cell biology 2008;10(5):611–8 doi: 10.1038/ncb1724[published Online First: Epub Date]|. [PubMed: 18391940]

15. Beloribi-Djefaflia S, Vasseur S, Guillaumond F. Lipid metabolic reprogramming in cancer cells. Oncogenesis 2016;5:e189 doi: 10.1038/oncsis.2015.49[published Online First: Epub Date]|. [PubMed: 26807644]

16. Zaidi N, Lupien L, Kuemmerle NB, Kinlaw WB, Swinnen JV, Smans K. Lipogenesis and lipolysis: the pathways exploited by the cancer cells to acquire fatty acids. Progress in lipid research 2013;52(4):585–9 doi: 10.1016/j.plipres.2013.08.005[published Online First: Epub Date]|. [PubMed: 24001676]

17. Lee JE, Wang C, Xu S, et al. H3K4 mono- and di-methyltransferase MLL4 is required for enhancer activation during cell differentiation. Elife 2013;2:e01503 doi: 10.7554/eLife.01503[published Online First: Epub Date]|. [PubMed: 24368734]

18. Kantidakis T, Saponaro M, Mitter R, et al. Mutation of cancer driver MLL2 results in transcription stress and genome instability. Genes Dev 2016;30(4):408–20 doi: 10.1101/gad.275453.115[published Online First: Epub Date]|. [PubMed: 26883360]

19. Guo C, Chang CC, Wortham M, et al. Global identification of MLL2-targeted loci reveals MLL2's role in diverse signaling pathways. Proceedings of the National Academy of Sciences of the United States of America 2012;109(43):17603–8 doi: 10.1073/pnas.l208807109[published Online First: Epub Date]|. [PubMed: 23045699]

20. Lee S, Lee J, Lee SK, Lee JW. Activating signal cointegrator-2 is an essential adaptor to recruit histone H3 lysine 4 methyltransferases MLL3 and MLL4 to the liver X receptors. Molecular endocrinology (Baltimore, Md.) 2008;22(6):1312–9 doi: 10.1210/me.2008-0012[published Online First: Epub Date]|.

21. Lee J, Saha PK, Yang QH, et al. Targeted inactivation of MLL3 histone H3-Lys-4 methyltransferase activity in the mouse reveals vital roles for MLL3 in adipogenesis. Proceedings of the National Academy of Sciences of the United States of America 2008;105(49):19229–34 doi: 10.1073/pnas.0810100105[published Online First: Epub Date]|. [PubMed: 19047629]

22. Kim DH, Kim J, Kwon JS, et al. Critical Roles of the Histone Methyltransferase MLL4/KMT2D in Murine Hepatic Steatosis Directed by ABL1 and PPARgamma2. Cell reports 2016;17(6):1671–82 doi: 10.1016/j.celrep.2016.10.023[published Online First: Epub Date]|. [PubMed: 27806304]

23. Hezel AF, Bardeesy N. LKB1; linking cell structure and tumor suppression. Oncogene 2008;27(55):6908–19 doi: 10.1038/onc.2008.342[published Online First: Epub Date]|. [PubMed: 19029933]

24. Spicer J, Ashworth A. LKB1 kinase: master and commander of metabolism and polarity. Current biology: CB 2004;14(10):R383–5 doi: 10.1016/j.cub.2004.05.012[published Online First: Epub Date]|. [PubMed: 15186763]

25. Ortega-Molina A, Boss IW, Canela A, et al. The histone lysine methyltransferase KMT2D sustains a gene expression program that represses B cell lymphoma development. Nature medicine 2015;21(10):1199–208 doi: 10.1038/nm.3943[published Online First: Epub Date]|.

26. Kroemer G, Pouyssegur J. Tumor cell metabolism: cancer's Achilles' heel. Cancer cell 2008;13(6):472–82 doi: 10.1016/j.ccr.2008.05.005[published Online First: Epub Date]|. [PubMed: 18538731]

27. Reske SN, Grillenberger KG, Glatting G, et al. Overexpression of glucose transporter 1 and increased FDG uptake in pancreatic carcinoma. Journal of nuclear medicine : official publication, Society of Nuclear Medicine 1997;38(9):1344–8

28. Ito H, Duxbury M, Zinner MJ, Ashley SW, Whang EE. Glucose transporter-1 gene expression is associated with pancreatic cancer invasiveness and MMP-2 activity. Surgery 2004;136(3):548–56 doi: 10.1016/j.surg.2004.05.032[published Online First: Epub Date]|. [PubMed: 15349101]

29. Simpson IA, Dwyer D, Malide D, Moley KH, Travis A, Vannucci SJ. The facilitative glucose transporter GLUT3: 20 years of distinction. Am J Physiol Endocrinol Metab 2008;295(2):E242–53 doi: 10.1152/ajpendo.90388.2008[published Online First: Epub Date]|. [PubMed: 18577699]

30. Flavahan WA, Wu Q, Hitomi M, et al. Brain tumor initiating cells adapt to restricted nutrition through preferential glucose uptake. Nature neuroscience 2013;16(10):1373–82 doi: 10.1038/nn.3510[published Online First: Epub Date]|. [PubMed: 23995067]

31. Yamamoto T, Seino Y, Fukumoto H, et al. Over-expression of facilitative glucose transporter genes in human cancer. Biochem Biophys Res Commun 1990;170(1):223–30 [PubMed: 2372287]

32. Kim JH, Sharma A, Dhar SS, et al. UTX and MLL4 coordinately regulate transcriptional programs for cell proliferation and invasiveness in breast cancer cells. Cancer research 2014;74(6):1705–17 doi: 10.1158/0008-5472.can-13-1896[published Online First: Epub Date]|. [PubMed: 24491801]

33. Guo C, Chen LH, Huang Y, et al. KMT2D maintains neoplastic cell proliferation and global histone H3 lysine 4 monomethylation. Oncotarget 2013;4(11):2144–53 doi: 10.18632/oncotarget.l555[published Online First: Epub Date]|. [PubMed: 24240169]

34. Lee J, Kim DH, Lee S, et al. A tumor suppressive coactivator complex of p53 containing ASC-2 and histone H3-lysine-4 methyltransferase MLL3 or its paralogue MLL4. Proceedings of the National Academy of Sciences of the United States of America 2009;106(21):8513–8 doi: 10.1073/pnas.0902873106[published Online First: Epub Date]|. [PubMed: 19433796]

35. Zhang J, Dominguez-Sola D, Hussein S, et al. Disruption of KMT2D perturbs germinal center B cell development and promotes lymphomagenesis. Nature medicine 2015;21(10):1190–8 doi: 10.1038/nm.3940[published Online First: Epub Date]|.

36. Dawkins JB, Wang J, Maniati E, et al. Reduced Expression of Histone Methyltransferases KMT2C and KMT2D Correlates with Improved Outcome in Pancreatic Ductal Adenocarcinoma. Cancer research 2016;76(16):4861–71 doi: 10.1158/0008-5472.can-16-0481[published Online First: Epub Date]|. [PubMed: 27280393]

37. Baenke F, Peck B, Miess H, Schulze A. Hooked on fat: the role of lipid synthesis in cancer metabolism and tumour development. Disease models & mechanisms 2013;6(6):1353–63 doi: 10.1242/dmm.011338[published Online First: Epub Date]|. [PubMed: 24203995]

38. Swierczynski J, Hebanowska A, Sledzinski T. Role of abnormal lipid metabolism in development, progression, diagnosis and therapy of pancreatic cancer. World journal of gastroenterology 2014;20(9):2279–303 doi: 10.3748/wjg.v20.i9.2279[published Online First: Epub Date]|. [PubMed: 24605027]

39. Tadros S, Shukla SK, King RJ, et al. De Novo Lipid Synthesis Facilitates Gemcitabine Resistance through Endoplasmic Reticulum Stress in Pancreatic Cancer. Cancer research 2017;77(20):5503–17 doi: 10.1158/0008-5472.can-16-3062[published Online First: Epub Date]|. [PubMed: 28811332]

40. Di Sebastiano KM, Yang L, Zbuk K, et al. Accelerated muscle and adipose tissue loss may predict survival in pancreatic cancer patients: the relationship with diabetes and anaemia. The British journal of nutrition 2013;109(2):302–12 doi: 10.1017/s0007114512001067[published Online First: Epub Date]|. [PubMed: 23021109]

41. Ebadi M, Mazurak VC. Evidence and mechanisms of fat depletion in cancer. Nutrients 2014;6(11):5280–97 doi: 10.3390/nu6115280[published Online First: Epub Date]|. [PubMed: 25415607]

Significance of this study

What is already known on this subject?

- Pharmacological targeting of epigenetic modifications contributes to uncovering therapeutic opportunities in pancreatic cancer.

- Several groups describe the deregulation and functional diversity of some histone methylation pathways in pancreatic adenocarcinomas.

- To date, the biological and translational significance of the aberrant function of the epigenetic regulators remains poorly understood, in particular for proteins controlling histone methylation.

What are the new findings?

- Transcriptional repression of *histone Lysine (K)-Specific Methyltransferase 2 (KMT2D)* is double-site CpG methylation-dependent.

- Pancreatic cancer growth is promoted by KMT2D downregulation.

- KMT2D suppression mediates loss of H3K4me3 signals in metabolic pathways and accounts for an induction of aerobic glycolysis and lipids' levels.

- SLC2A3 (also known as GLUT3) serves as a mediator of KMT2D-induced effects in cellular metabolic and proliferative rates.

- Pancreatic cancer patients harboring low *KMT2D* levels have worse prognosis and significant weight/BMI alterations.

How might it impact on clinical practice in the foreseeable future?

- Characterization of KMT2D-associated metabolic signatures provides a new molecular rationale to identify and develop a new generation of therapeutic agents.

- Future studies exploring the causal molecular link between KMT2D expression and clinical outcomes across the range of body weight and BMI may offer prognostic information and insights into pancreatic tumorigenesis and progression.
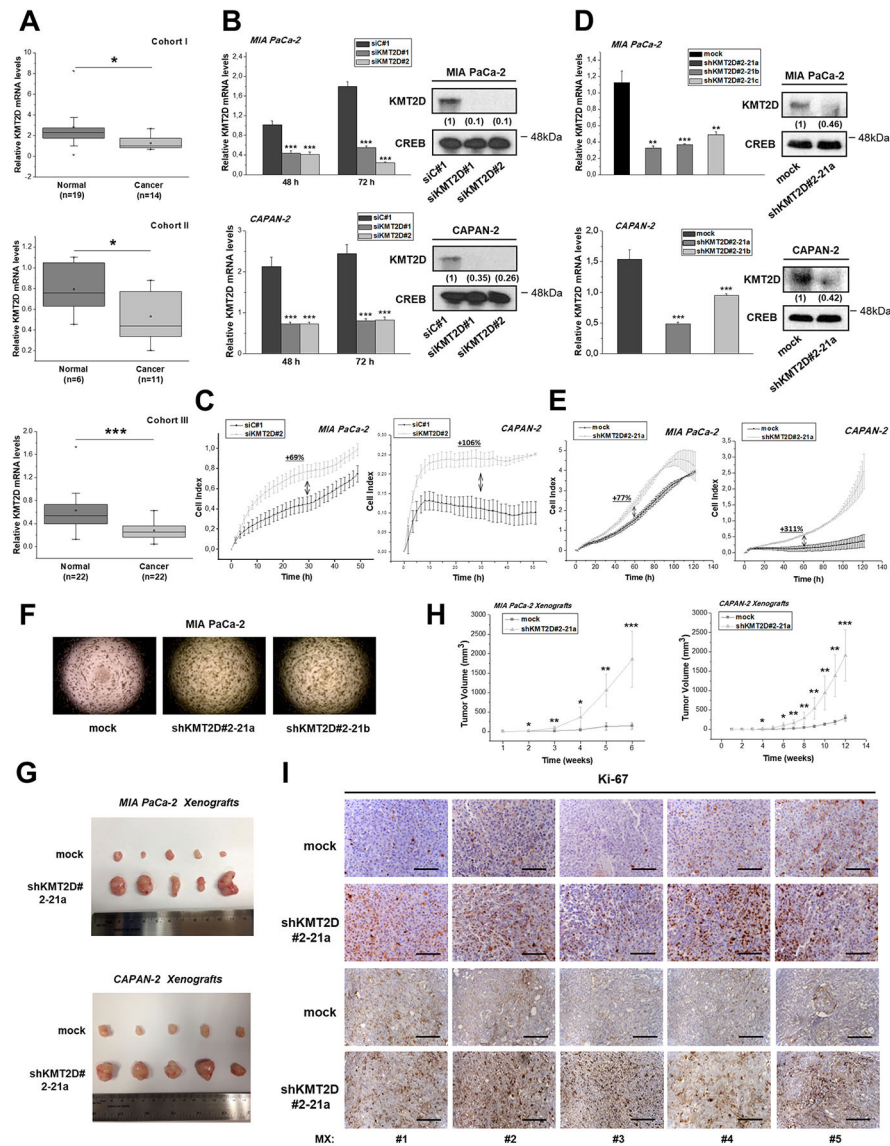
Figure 1. Histone methyltransferase KMT2D acts as a tumor suppressor in pancreatic cancer.
(**A**) KMT2D mRNA expression levels in 3 Cohorts of pancreatic cancer and normal tissues, as assessed by RT-qPCR. (**B**) Transient suppression of KMT2D expression by 2 different siRNAs in pancreatic cancer cells. Efficiency of KMT2D downregulation, as assessed by RT-qPCR (left panel) and by IB analysis (right panel). Whole cell protein extracts were analyzed by IB analysis for total KMT2D or CREB (used as a loading control). Numbers in parentheses denote the average-fold change of the ratio KMT2D:CREB total protein of siKMT2D-transiently transfected cells compared with siC#1-treated cells (set as default 1) of at least 2 independent experiments, as assessed by densitometric analysis of the immunoreactive bands. (**C**) Dynamic monitoring of cellular proliferation upon *KMT2D* transient suppression by using siKMT2D#2, using the xCELLigence RTCA SP system. (**D**) Assessment of KMT2D expression levels in MIA PaCa-2 cells transfected with #2–21 shRNA against KMT2D, that underwent clonal selection resulting in clones a, b and c, by

RT-qPCR (left panel) and IB analysis (right panel). Numbers in parentheses denote the average-fold change of the ratio KMT2D:CREB total protein of shKMT2D-stably transfected cells compared with mock-treated cells (set as default 1), as assessed by densitometric analysis of the immunoreactive bands. **(E)** Dynamic monitoring of the proliferation of the shKMT2D#2–21a clonal pancreatic cancer cell lines versus mock transfected cells. **(F)** Effect of KMT2D stable suppression on soft agar colony formation. (G) Representative images of the excised tumors and **(H)** tumor volume (mm^3) graphs of xenografts bearing KMT2D stably-suppressed MIA PaCa-2 and CAPAN-2 cells (n=5 mice per group). For establishing shKMT2D#2–21a xenografts, 3.5*10^6 MIA PaCa-2 or CAPAN-2 cells were injected subcutaneously in the right flank of NOD-SCID mice (5 mice/ group). **(I)** Representative IHC images for the proliferation marker Ki-67, corresponding to MIA PaCa-2 (upper 2 rows) and CAPAN-2 (bottom 2 rows) xenografts from mice injected with mock or shKMT2D#2–21a cells. Scale bars represent 50 μm. siC#1, cells transfected with a negative control scramble siRNA; siKMT2D#1, cells transfected with siRNA#1 for KMT2D; siKMT2D#2, cells transfected with siRNA#2 for KMT2D; mock, cells transfected with shRNA empty vector; shKMT2D#2–21, cells transfected with #2–21 shRNA for KMT2D; shKMT2D#2–21a, b or c, cells transfected with #2–21 shRNA for KMT2D that underwent clonal selection resulting in clones a, b and c; MX, Mouse Xenograft. OD, Optical Density. Statistical analyses were performed using one-way ANOVA. Asterisks denote statistically significant differences, * $P<.05$, ** $P<.01$, *** $P<.001$
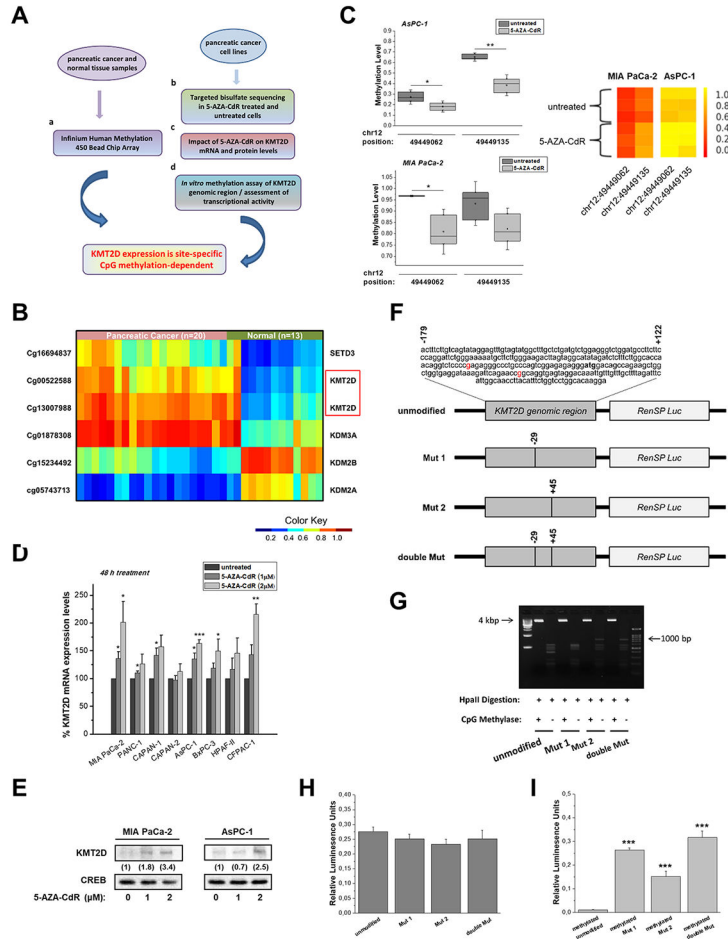
Figure 2. Epigenetic regulation of KMT2D levels through DNA methylation of 2 CpG sites.
(A) Experimental design for the evaluation of *KMT2D* transcriptional repression-
dependency on CpG methylation in pancreatic cancer. **(B)** Heatmap of methylation beta
values for the selected probes (*P<.05*, mean difference .25). Wilcoxon rank-sum tests were
conducted to compare methylation array data between pancreatic cancer patients and healthy
controls. **(C)** Validation of CpG methylation levels via Targeted Bisulfite Sequencing for the
selected ROI (chr12: 49448986–49449286). Quantitative methylation measurements at the
single-CpG-site level for untreated or 5-AZA-CdR-treated cells are box plotted (left panel)
or depicted as heatmaps of the methylation ratio (right panel). The color indicates the level
of methylation from higher to lower in yellow > orange > red order. **(D)** Dose response
evaluation of 5-AZA-CdR treatment for 48 h in KMT2D mRNA levels, as assessed by RT-
qPCR. **(E)** Effect of 5-AZA-CdR treatment for 48 h on KMT2D protein levels, as assessed
by IB analysis. Numbers in parentheses denote the average-fold change of the ratio
KMT2D:CREB total protein in 5-AZA-CdR-treated cells compared with .005% DMSO-
treated cells (set as default 1). **(F)** Schematic depiction of the distinct *KMT2D/hRluc*
constructs used; the engineered *hRluc* was coupled to the genomic region (positions −179 to
+121) of the human *KMT2D* gene. Tick marks represent the number and location of CpG
dinucleotides. **(G)** The efficiency of CpG methylation was assessed in unmethylated and

methylated, linearized and gel-purified constructs by resistance to digestion with Hpall endonuclease and subsequently agarose gel analysis. **(H, I)** Relative *hRluc* activity after *in vitro* methylation of *KMT2D* constructs using the promoterless pGL4.82 [*hRluc/*Puro] Vector gene system. *HRluc* mean fluorescence intensity was measured in MIA PaCa-2 cells transfected with either **(H)** untreated or **(I)** CpG methyltransferase (MSssl)-treated *KMT2D/ hRluc* constructs. To control for transfection efficiency, cells were cotransfected with a plasmid containing *firefly luciferase (Luc)* reporter gene and the levels of *hRluc* fluorescence were averaged over all *Luc* expressing cells. Statistical analyses were performed using oneway ANOVA. Asterisks denote statistically significant differences, * $P<.05$, ** $P<.01$, *** $P<.001$
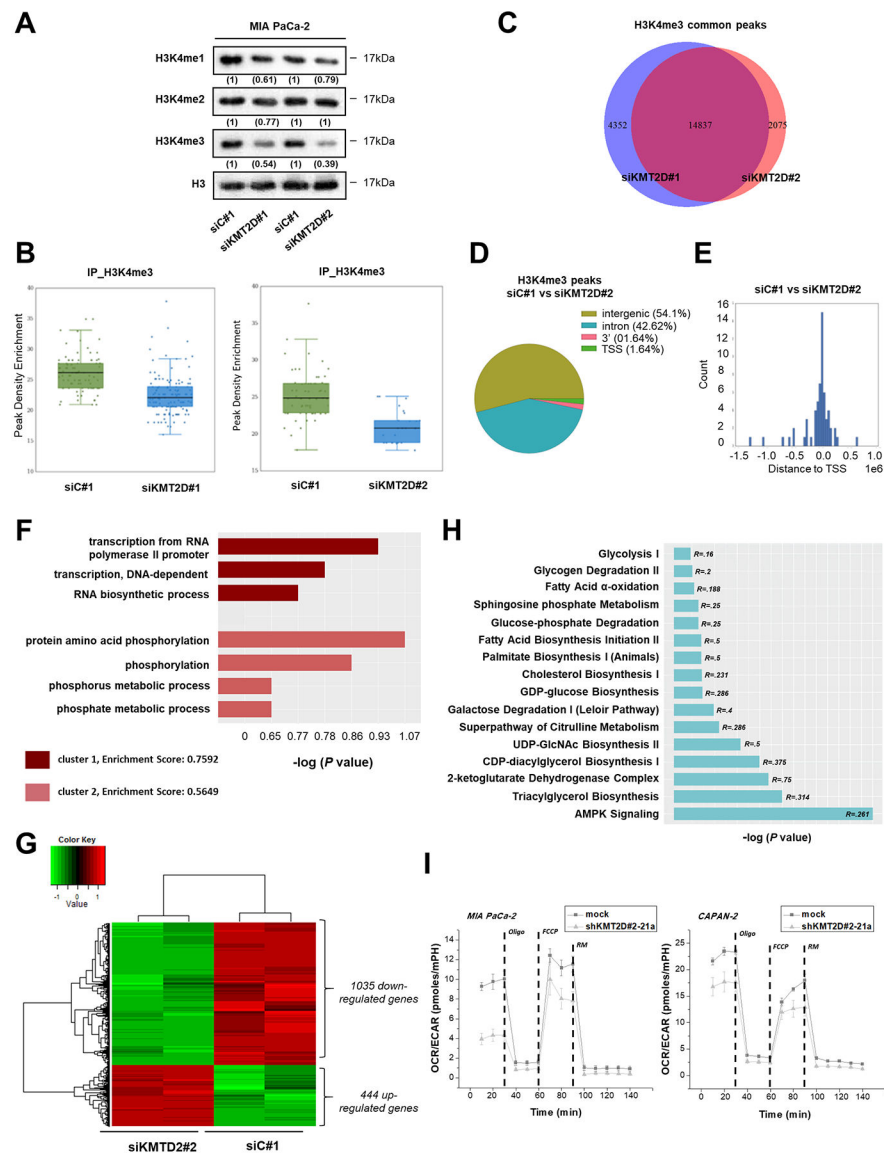
Figure 3. KMT2D-regulated pancreatic cancer cells' transcriptome and epigenome.
(A) Effects of KMT2D silencing on the global levels of histone H3K4 mono-, di- and tri-methylation using IB analysis. Numbers in parentheses denote the average-fold change of the ratio H3K4me1, H3K4me2, orH3K4me3:H3 total protein in *KMT2D*-silenced cells versus siC#1-treated cells (set as default 1). **(B)** Enrichment scores comparing the read density conditions for each set of peak regions are shown in the jittered boxplots. The enrichment values were tested with the Mann-Whitney U test (*P*<.001). **(C)** Overlap of H3K4me3 peaks upon KMT2D suppression using 2 different siRNAs. **(D)** Effect of *KMT2D* silencing on the genomic distribution of H3K4me3 peaks in MIA PaCa-2 cells. Pie chart indicates the enriched H3K4me3 peaks in negative siRNA versus siKMT2D#2 treated cells. **(E)** Distribution of H3K4 tri-methylation mark around TSS. **(F)** GO terms associated with H3K4me3 binding sites were determined as follows; ChIP-seq peaks found in siC#1 treated cells versus peaks found in cells treated with siKMT2D#2 were associated with the nearest

ENSEMBL transcript and processed using David (v6.7) tools. The data presented is log transformed P value of GO terms found to be enriched in the tested group of genes. **(G)** Heatmap showing the differentially expressed genes in MIA PaCa-2 cells upon *KMT2D* suppression. Data was filtered using a *P* value cutoff of .05 and a fold change cut-off of 2.0. Clustering dendrograms show the relative expression values according to the following coloring scheme: red = high, black=moderate, green=low. **(H)** List of metabolism-associated canonical pathways derived from Ingenuity Pathway Analysis (IPA) GO algorithms for the KMT2D-regulated genes (from Figure 3G). -log (P value) is measured by the bar length, while R refers to the number of molecules from the dataset that map to the pathway listed divided by the total number of molecules that map to the pathway from within the IPA knowledge base. **(I)** OCR/ECAR curves for KMT2D stably-transfected pancreatic cancer cells (Seahorse technology). *R*, Ratio; Oligo, Oligomycin; FCCP, Carbonyl cyanide-4-(trifluoromethoxy) phenylhydrazone; RM, Rotenone/Myxothiazol.
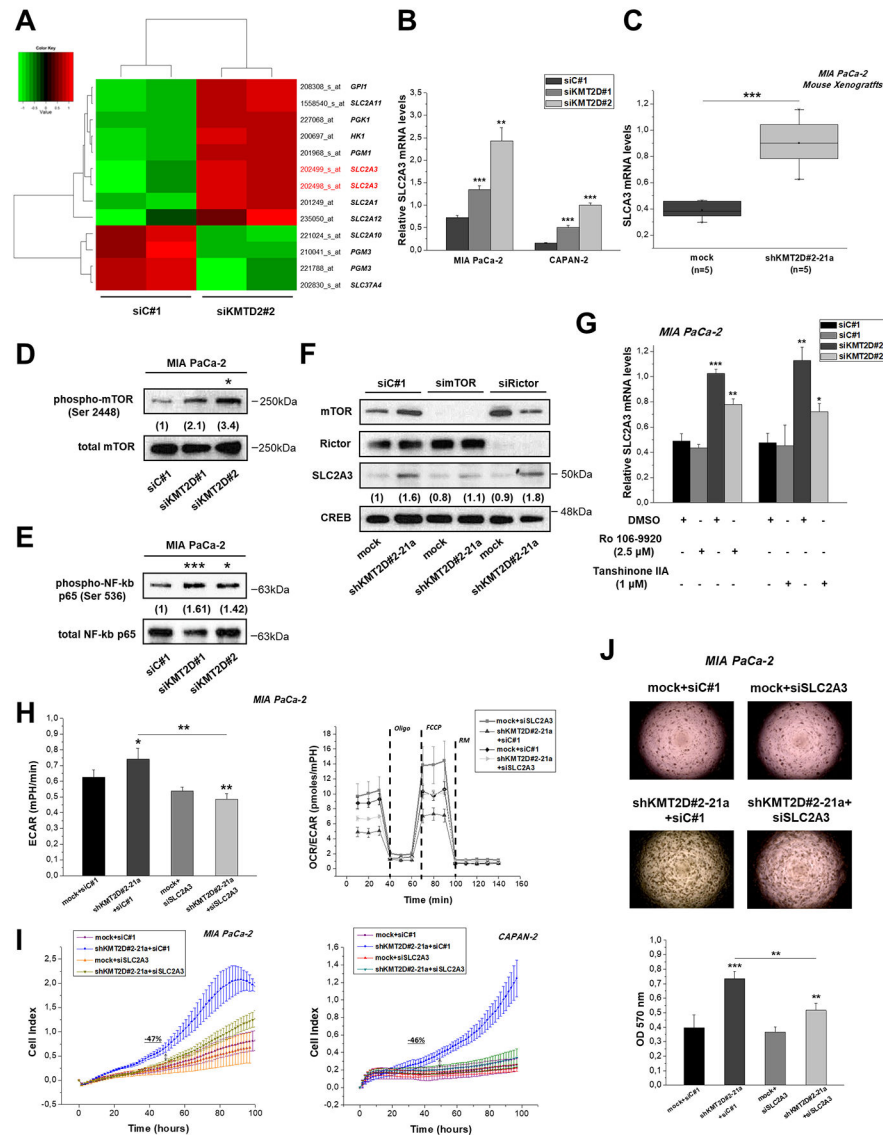
Figure 4. KMT2D regulates pancreatic cancer cell growth and metabolism by affecting SLC2A3 glucose transporter.

(**A**) Heatmap summarizing the differentially expressed glycolysis-related genes in MIA PaCa-2 cells upon KMT2D suppression. Data was filtered using a *P* value cutoff of .05 and a fold change cut-off of 1.25. (**B**) SLC2A3 mRNA expression in pancreatic cancer cells upon KMT2D silencing. (**C**) *SLC2A3* expression in MIA PaCa-2 xenografts from mice injected with mock or shKMT2D#2–21a cells, as assessed by RT-qPCR. (**D**) Representative IB images for the activated and total (**D**) mTOR and (**E**) NF-kB p65 upon KMT2D silencing. Numbers in parentheses denote the average-fold change of the ratio phosphorylated: total protein of *KMT2D*-silenced cells versus siC#1-treated cells (set as default 1) of at least 2 independent experiments. (**F**) Representative IB images for SLC2A3, mTOR, Rictor and CREB protein levels upon treatment of MIA PacA-2 cells harboring differential KMT2D levels with siRNAs against mTOR, Rictor or the respective scramble control. Numbers in parentheses denote the average-fold change of the ratio SLC2A3:CREB total protein of

siRNA-treated cells versus siC#1-treated cells (set as default 1). **(G)** Treatment of MIA PaCa-2 cells with inhibitors of NF-kB activation for 24 h reverses the KMT2D-mediated increase in SLC2A3 mRNA levels. Effects of SLC2A3 silencing on the **(H)** bioenergetic status, **(I)** proliferation and **(J)** colony formation ability of KMT2D-suppressed cells. Statistical analyses were performed using one-way ANOVA. Asterisks denote statistically significant differences, * $P<.05$, ** $P<.01$, *** $P<.001$
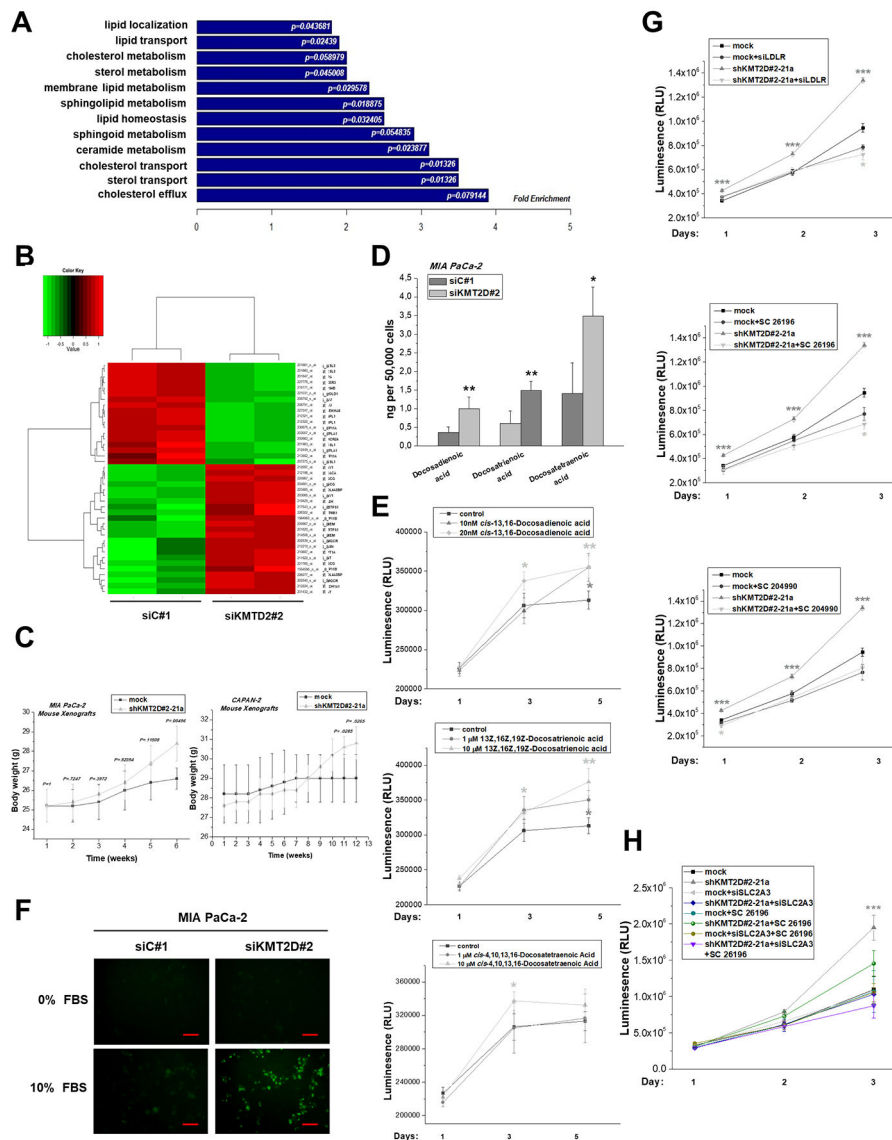
Figure 5. KMT2D inhibition alters the lipid composition and cholesterol content in pancreatic cancer.

(**A**) GO-based annotation was used to perform functional enrichment analysis using the DAVID (v6.7) tools. Fold enrichment of genes (associated to lipid metabolic processes) regulated by KMT2D levels is measured by the bar length while *P* value represents the significance of the enrichment. (**B**) Heatmap summarizing the differentially expressed lipid metabolism-related genes in MIA PaCa-2 cells upon KMT2D suppression. Data was filtered using a *P* value cutoff of .05 and a fold change cut-off of 1.5. (**C**) Body weight graphs of mouse xenografts bearing MIA PaCa-2 or CAPAN-2 shKMT2D#2–21a clonal cell lines and mock-transfected cells (n=5 mice per group). (**D**) Column graph illustrating quantitative changes of the top 3 FAs regulated by KMT2D. (**E**) Time- and dose-dependent effect of exogenously added FAs on cell proliferation, as assessed by CellTiter Glo Luminescence Cell Viability Assay. (**F**) Detection of cholesterol uptake within MIA PaCa-2 cultured cells, as assessed by fluorescence microscopy. Scale bars represent 50 μm. (**G, H**) Time-dependent
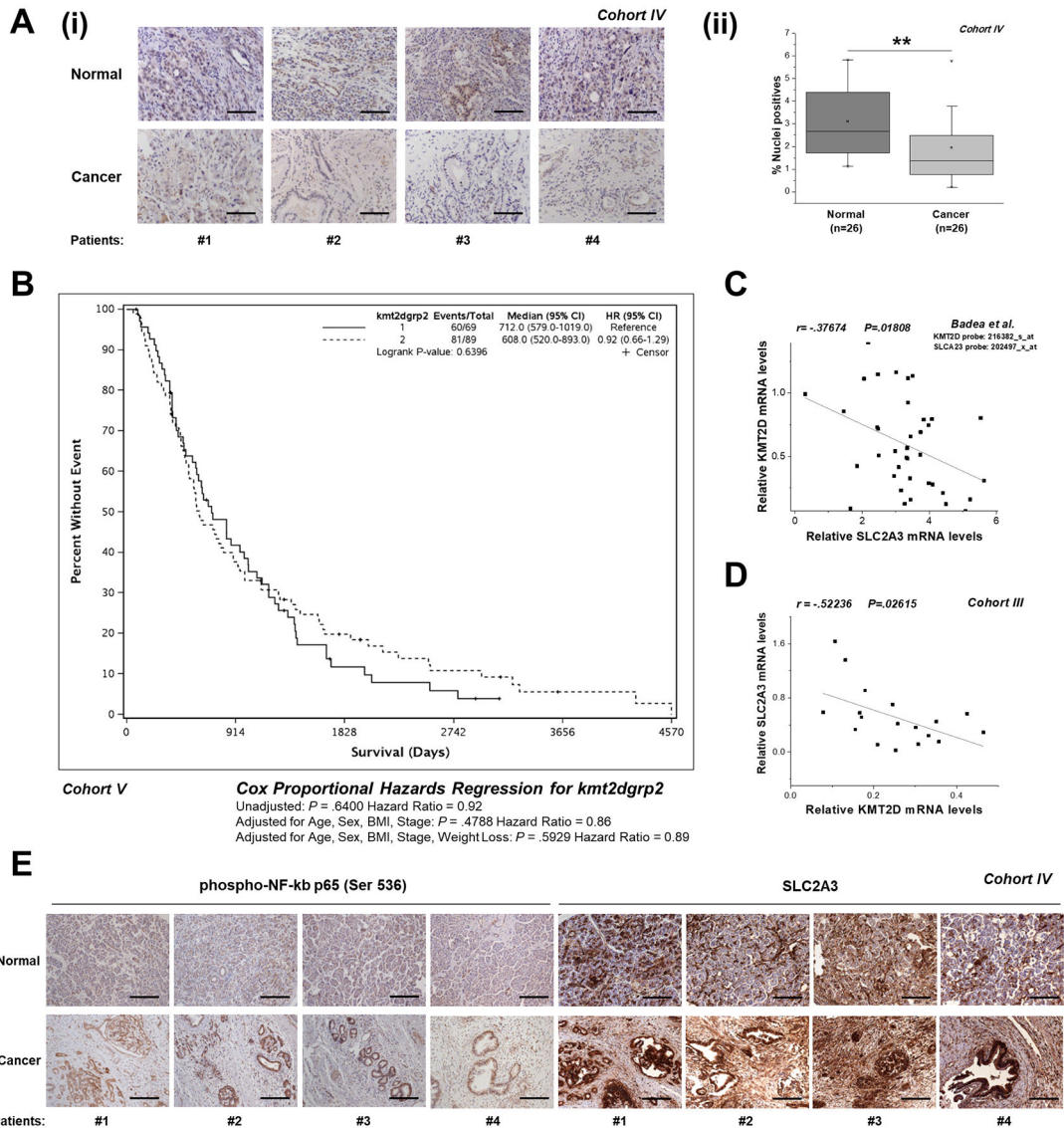
effect of LDLR or SLC2A3 silencing, SC 26196 and SC 204990 inhibitors on cell proliferation in high and low KMT2D-expressing cells, as assessed by CellTiter Glo Luminescence Cell Viability Assay. Statistical analyses were performed using one-way ANOVA. Asterisks denote statistically significant differences, * $P<.05$, ** $P<.01$, *** $P<.001$

Figure 6. Correlation of KMT2D levels between its targets and disease aggressiveness.
(A) (i) Representative images (10x magnification) of KMT2D expression, as assessed by IHC analysis, in matched cancer and normal tissues from pancreatic cancer patients (Cohort IV). **(ii)** Automated image analysis using the Spectrum Software V11.1.2.752 (Aperio) was performed for nuclear staining quantification. **(B)** Correlation of *KMT2D* expression with overall patient survival. Kaplan-Meier survival curves of patients harboring below median (<3.917) and above median (>3.917) *KMT2D* levels derived from Cohort V. **(C, D)** Correlation of *KMT2D* levels with *SLC2A3* expression in pancreatic cancer patients based on the study by Badea et al., 2008 [4] and as assessed by RT-qPCR (Cohort III). **(E)** Representative images (10x magnification) of phospho-NF-kB p65 (Ser 536) and SLC2A3 expression, as assessed by IHC analysis, in matched cancer and normal tissues from pancreatic cancer patients (Cohort IV). Scale bars represent 50 μm. *r*, Pearson correlation coefficient; The Kaplan-Meier test was used for univariate survival analysis. The Cox

proportional hazard model was used for multivariate analysis and for determining the 95% confidence interval. Statistical analyses were performed using one-way ANOVA or Pearson correlation. Asterisks denote statistically significant differences, ** $P<.01$
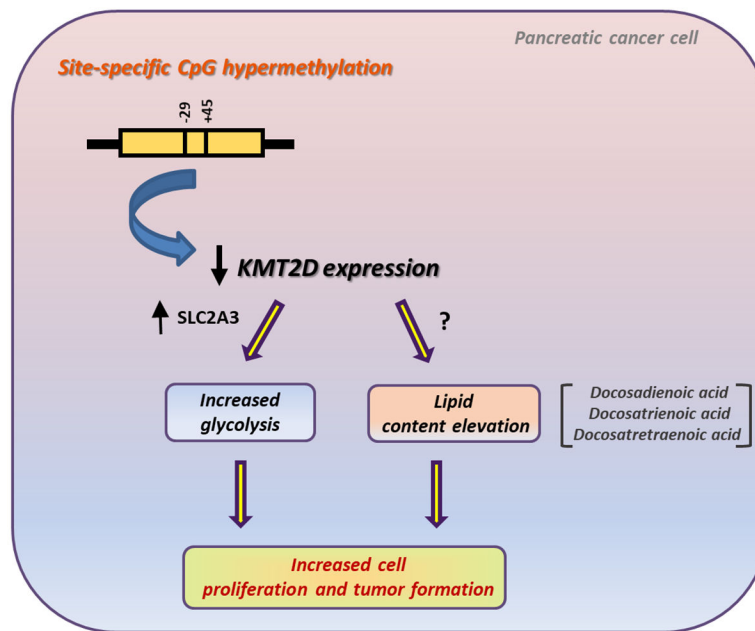
Figure 7. Schematic depiction of KMT2D transcriptional regulation and downstream mechanistic targets and pathways in pancreatic cancer.
Methylation of 2 single CpG sites transcriptionally represses KMT2D histone methyltransferase expression. Suppression of KMT2D induces aerobic glycolysis and lipid levels in pancreatic cancer. SLC2A3 consists a key mediator of the cellular growth and metabolic effects triggered by KMT2D downregulation. Docosadienoic, docosatrienoic and docosatetraenoic acid represent the top KMT2D-regulated FAs and harbor oncogenic properties in pancreatic cancer cells.

Table 1

Effect of KMT2D silencing on the lipidomic profile of pancreatic cancer cells.

Quantitative LC-MS data of FAs and total cholesterol in MIA PaCa-2 cells pretreated with siC#1 or siKMT2D#2. The top 3 lipids, most significantly elevated by KMT2D reduction, are shown in bold. Statistical analyses were performed using one-way ANOVA.

Lipid	siC#1 (ng) per 50,000 cells	siKMT2D#2 (ng) per 50,000 cells	% percentage change	*P* value
Docosatrienoic acid	.6	1.5	+150	.00482
Docosadienoic acid	.35	1	+186	.00971
Docosatretraenoic acid	1.425	3.5	+150	.01084
Nervonic acid	4.1	10.1	+146.3	.00217
Eicosadienoic acid	2.825	6.55	+131.8	.00557
Dihomo-g-linolenic acid	1.3	2.925	+125	.0075
Eicosapentaenoic acid	8	17.075	+113.4	.19345
Eicosenoic acid	32.675	68.675	+110.2	.00116
Docosapentaenoic acid (n=3)	4.55	9.1	+100	.000229
Docosenoic acid	3.65	6.825	+87	.00364
Docosahexaenoic acid	4.675	8.2	+75.4	.02643
Arachidonic acid	8.933	13.825	+54.8	.009
g-Linolenicacid	8.325	12.175	+46.2	.16032
Oleic acid	715.6	1049.775	+46.7	.01402
a-Linolenic acid	4.1	5.9	+43.9	.16846
Stearic acid	2563.2	3667.875	+43.1	.11082
Linoleic acid	23.7	33.575	+41.7	.07341
Hexacosanoic acid	7.05	9.95	+41.1	.13026
Cholesterol	359.25	474.75	+32.2	.04811
Dodecanoic acid	82.25	108.1	+31.4	.0013
Palmitoleic acid	118.775	148.575	+25.1	.26513
Lignoceric acid	25.375	30.825	+21.5	.21665
Palmitic acid	7676	8941.525	+16.5	.05763
Docosanoic (Behenic acid)	9.575	10.475	+9.4	.38668
Heptadecenoic acid	71.55	78.075	+9.1	.10477
Pentadecanoic	486.375	524.125	+7.8	.27158
Heptadecanoic acid	91.15	96.85	+6.3	.35989
Arachidic acid	20.55	21.65	+5.4	.5251
Myristic acid	459.625	480.375	+4.5	.08533

Table 2

Correlation of KMT2D expression with demographic and clinical characteristics of pancreatic cancer patients (Cohort V).

Pancreatic carcinomas were subdivided in 2 groups: carcinomas with below median (<3.917) *KMT2D* expression and carcinomas with above median (>3.917) *KMT2D* expression. N: number of patients with clinical information; BMI: Body Mass Index. Clinical correlations were examined using the SAS software.

KMT2D Expression	Below Median (3.917) (N=109)	Above Median (>3.917) (N=111)	*P* value
Age at Diagnosis			.4976
N	86	102	
Mean (SD)	64.65 (11.72)	64.01 (11.53)	
Median	66.50	63.50	
Q1, Q3	55.00, 75.00	57.00, 74.00	
Range	(37.00–88.00)	(41.00–92.00)	
Vital Status			.1274
Missing	10	5	
Alive	14 (14.1%)	8 (7.5%)	
Deceased	85 (85.9%)	98 (92.5%)	
Survival (Days)			
N	69	89	
Events	60	81	
Median Survival Days	712.0 (552.0–1017.0)	608.0 (518.0–811.0)	
5 Yr Survival Rate	11.7% (3.5%–20.0%)	19.7% (11.3%–28.2%)	
Year 5 N at Risk	6	15	
Sex			.2999
Missing	10	5	
Female	52 (52.5%)	48 (45.3%)	
Male	47 (47.5%)	58 (54.7%)	
Race			.3702
Missing	14	5	
1=American Indian/Alaskan N ative	0 (0.0%)	1 (0.9%)	
2=Asian/Asian-American	2 (2.1%)	0 (0.0%)	
3=Black/African-American	1 (1.1%)	1 (0.9%)	
5=White	92 (96.8%)	104 (98.1%)	
Usual Adult BMI			.0040
N	74	95	
Mean (SD)	27.31 (5.40)	29.92 (5.64)	
Median	27.01	29.19	
Q1, Q3	24.24, 30.04	25.75, 32.96	
Range	(15.31–43.72)	(18.88–46.18)	
Usual Adult BMI (<30,30+)			.0367
Missing	35	16	
<30	55 (74.3%)	56 (58.9%)	

KMT2D Expression	Below Median (3.917) (N=109)	Above Median (>3.917) (N=111)	*P* value
30+	19 (25.7%)	39 (41.1%)	
Weight Loss			.0005
Missing	10	5	
No	43 (43.4%)	22 (20.8%)	
Yes	56 (56.6%)	84 (79.2%)	
Pounds Lost			.0001
N	99	106	
Mean (SD)	11.28 (13.65)	20.65 (18.35)	
Median	5.95	17.50	
Q1, Q3	0.00, 20.00	9.92, 30.00	
Range	(0.00–60.00)	(0.00–85.00)	
Stage at Surgery			.3117
Missing	49	26	
IA	0 (0.0%)	1 (1.2%)	
IB	6 (10.0%)	6 (7.1%)	
IIA	12 (20.0%)	28 (32.9%)	
IIB	42 (70.0%)	49 (57.6%)	
IV	0 (0.0%)	1 (1.2%)	

Table 3

Lipidomic profiling of low-KMT2D expressing pancreatic cancer biopsies versus normal pancreata.

Quantitative LC-MS data of FAs and total cholesterol in pancreatic cancer biopsies versus normal tissues. Pancreatic carcinomas from Cohort II were subdivided in 2 groups: carcinomas with below median (<.3) *KMT2D* expression and carcinomas with above median (>.3) *KMT2D* expression. 4 cancerous tissues displaying below median (<.3) *KMT2D* levels underwent Lipidomic Profiling. The top 3 lipids, most significantly elevated are shown in bold. Statistical analyses were performed using one-way ANOVA.

Lipid	Adjacent Normal	Cancerous Tissue	% percentage change	*P* value
Docosatrienoic acid	-	.0125	∞	.04006
Docosadienoic acid	-	.0225	∞	.02401
Docosatretraenoic acid	.0325	.2125	+553.8	.03181
Nervonic acid	.05	.275	+450	.07178
Eicosadienoic acid	.0475	.6325	+1232	.06733
Dihomo-g-linolenic acid	.075	.34	+353	.03279
Eicosapentaenoic acid	.085	.1125	+32.35	.64401
Eicosenoic acid	1.0775	13.371	+1426.2	.06179
Docosapentaenoic acid (n=3)	.045	.2025	+350	.08372
Docosenoic acid	.2375	1.34	+464.21	.03204
Docosahexaenoic acid	.055	.1625	+195.45	.09208
Arachidonic acid	.695	1.32	+89.93	.07636
Oleic acid	36.4525	347.835	+854.2	.13282
a&g-Linolenic acid	.0225	.315	+1300	.05199
Stearic acid	15.275	20.23	+32.94	.59416
Linoleic acid	3.1525	15.5675	+393.8	.09712
Hexacosanoic acid	.0125	.0225	+80.0	.71105
Cholesterol	23.28843	53.64114	+130.33	.00787
Dodecanoic acid	.5075	1.87	+268	.03587
Palmitoleicacid	3.515	29.14	+788	.09423
Lignoceric acid	.12	.27	+125	.29288
Palmitic acid	25.89	59.3875	+129.4	.17425
Docosanoic (Behenic acid)	.13	.2725	+109.62	.02932
Heptadecenoic acid	.4525	3.64	+704	.10735
Pentadecanoic	.34	1.86	+447.1	.06233
Heptadecanoic acid	.33	1.72	+421.2	.06334
Arachidic acid	.14	.5875	+319.64	.02278
Myristic acid	1.5275	10.325	+675.9	.05614